PASJ: Publ. Astron. Soc. Japan **49**, 17–46 (1997)

Nuclear-to-Outer Rotation Curves of Galaxies in the CO and H I Lines

Yoshiaki SOFUE
Institute of Astronomy, Faculty of Science, The University of Tokyo, 2-21-1 Osawa, Mitaka, Tokyo 181
E-mail: sofue@mtk.ioa.s.u-tokyo.ac.jp

(Received 1996 September 13; accepted 1996 November 14)

Abstract

We have derived rotation curves of nearby galaxies, which are almost completely sampled from the inner to outer regions. We used high-resolution position–velocity diagrams in the CO line along the major axes for the inner regions, and H I-line data for the outer regions. We combined the CO and H I data to obtain total rotation curves from the nuclear to outer regions. The rotation curves show a steep nuclear rise within a radius smaller than the resolutions of the CO-line observations, indicating a compact massive concentration near the nucleus. We show that the nuclear steep rise is general and universal, and that a rigid body-like gentle rise is exceptional.

Key words: Galaxies: general — Galaxies: kinematics — Galaxies: rotation — Galaxies: structure — ISM: CO emission — ISM: H I gas

1. Introduction

Rotation curves (RC) of galaxies obtained by optical (Hα) and H I 21-cm line observations have been known to show a rigid-body like increase in the central few kpc region, followed by a flat rotation in the disk and outer regions (Rubin et al. 1980, 1982; Bosma 1981b; Persic et al. 1995). Since the H I gas is widely distributed in the galactic disk, even extending to the edges of galaxies, H I rotation curves are most useful for investigating the mass distribution in the outer region, and have been used to study the massive dark halo (Kent 1987). On the other hand, the H I gas is deficient in the central region, where the molecular hydrogen dominates (Sofue et al. 1994). CO-line observations have been obtained for a large number of galaxies during the last decade (Young, Scoville 1992), and position–velocity diagrams for the central region of these galaxies have been obtained. The CO rotation curves for the nuclear regions have suggested a much sharper rise in the central few hundred parsecs than has been found based on H I or optical observations, which has been indeed observed for the Milky Way Galaxy (Clemens 1985).

Combining the CO-line rotation curves for the central regions with H I and optical RC in the outer disks, we have obtained the 'most completely sampled rotation curves' for several nearby galaxies (Sofue 1996; Paper I). The radio (CO+H I) rotation curves are found to have a sharp nuclear rise, often associated with a high-velocity peak, in the central few hundred parsecs, then a gap followed by a second maximum at 5 to 10 kpc, and a flatter or slowly declining outer part.

In this paper, we present radio (CO+H I) and optical rotation curves for a larger number of spiral galaxies using high-resolution CO and H I-line data. We aim at clarifying whether the nuclear rise of rotation curves is indeed a universal and general characteristic of the rotation of spiral galaxies.

2. Envelope-Tracing Method for Deriving Rotation Curves

We adopt the envelope-tracing method, as used in Paper I, to derive rotation curves, which uses the loci of terminal velocity in position–velocity (PV) diagrams. We define the terminal velocity by a velocity at which the intensity becomes equal to

$$I_{\rm t} = [(0.2\, I_{\rm max})^2 + I_{\rm lc}^2]^{1/2} \tag{1}$$

on the PV diagrams, where $I_{\rm max}$ and $I_{\rm lc}$ are the maximum intensity and intensity corresponding to the lowest contour level, respectively. This equation defines a 20% level of the intensity profile at a fixed position, $I_{\rm t} \simeq 0.2 \times I_{\rm max}$, if the signal-to-noise ratio is sufficiently high. If the intensity is not high enough, the equation gives $I_{\rm t} \simeq I_{\rm lc}$, which approximately defines the loci along the lowest contour level ($\sim 3 \times$ rms noise). The terminal velocity is then corrected for the velocity dispersion of the interstellar gas ($\sigma_{\rm ISM}$) and the velocity resolution of observations ($\sigma_{\rm obs}$) as

$$V_{\rm t}^0 = V_{\rm t} - (\sigma_{\rm obs}^2 + \sigma_{\rm ISM}^2)^{1/2}. \tag{2}$$

Small-scale structures due to clumpy ISM and clouds, and partly due to the noise in the observations, are smoothed by eye estimates. Since it was not practical to apply these procedures automatically by a computer, we drew the curves by hand on each position–velocity diagram. The rotation velocity is finally obtained by

$$V_{\rm rot} = V_{\rm t}^0 / \sin\ i, \tag{3}$$

where i is the inclination angle of the disk plane. The accuracy of determining the terminal velocity, and therefore the accuracy of the obtained rotation curve, was typically ± 10–$15/\sin\ i$ km s^{-1}.

Simply-traced envelopes on the two sides of the nucleus have a discontinuity at the nucleus due to the finite beam width. We avoided this discontinuity by stopping the tracing at a radius corresponding to the telescope resolution, and then by connecting both sides of the rotation curve by a straight (solid-body like) line crossing the nucleus at zero velocity. Figure 1 shows examples of the CO-line position–velocity diagrams and traced rotation curves for several galaxies, combined with H I rotation curves. The pair of rotation curves thus obtained on both (receding and approaching) sides of the nucleus are finally averaged to give a rotation curve as a function of the radius. The inner rotation curves thus derived from CO-line data were then connected smoothly to the H I curves in the outer disk. In most cases the discrepancy between the CO and H I rotation velocities at the connecting area were within about ± 10 km s^{-1}. Since the CO data usually have a higher resolution than H I, we adopted CO curves when both CO and H I curves were available at the same radius.

3. CO+H I Rotation Curves for Individual Galaxies

Figure 2 shows the obtained radio (CO+H I) rotation curves for the studied galaxies with the basic data inserted, such as the inclination, position angle of the major axis, and a possible distance taken from the literature cited in table 1. Since these distances are often uncertain, the linear scales indicated along the upper ordinates are also uncertain. The vertical bars of the crosses represent the typical errors in the velocity determination, and the horizontal bars indicate the angular resolutions of the observations. The vertical dashed lines separate each rotation curve into two or three parts, where the CO and H I data have been used, respectively. When different data with different angular resolutions are combined, their border is also indicated by a dashed line. We show this by inset optical images of the galaxies taken from the STScI Digitized Sky Survey (DSS). A $10' \times 10'$ field is displayed for each object (larger fields for a few galaxies), and the angular scale is given along the major axis. We describe the individual galaxies below. The parameters and references for the data are listed in table 1.

NGC 224 (M31): This galaxy is one of the few exceptional nearby galaxies of the Sb type, which emit very weak CO line emission in the center. Even in our deep observation with the Nobeyama 45-m telescope we could detect only weak, or almost no, CO emission in the nuclear region (Sofue, Yoshida 1993). Therefore, no sufficient kinematical data are available to derive a CO rotation curve. However, there have been a number of studies of the rotation curve, as summarized in Sofue and Kato (1981). We revisited and obtained a new RC using the optical data in the [N II] λ6583 emission observed by Rubin and Ford (1970) and in the Hα line by Ciardullo et al. (1988). We adopted the Hα velocities for the very inner region within $1'$, and those from [N II] line for the inner $6'$, where the rotation rises steeply to a peak velocity of 220 km s^{-1} at $2'$ radius. Beyond this radius, we adopted the H I data from the Bonn 100-m telescope, which is sensitive enough to trace the rotation with a sufficient accuracy, although the resolution ($9'$) was not enough to resolve the innermost region. The H I position–velocity diagram shows a pair of symmetrical shoulders at $\pm 10'$ with respect to the nucleus, corresponding to the central peak indicated by the optical observations. The velocity, then, increases to a maximum as high as 280 km s^{-1} at $40'$, and declines slowly toward the edge.

NGC 253: This is a CO-rich starburst galaxy, and has been studied in Paper I based on a lower-resolution CO data. We revisited this galaxy using the higher-resolution CO data from the 45-m telescope. The central peak of the rotation curve is more clearly seen in the new data. See Paper I.

IC 342: A central rise and a step, corresponding to the nuclear peak at 130 km s^{-1}, is followed by an almost flat rotation in the disk and outer part. See Paper I.

NGC 598 (M33): Because of its proximity, we used lower-resolution CO data from the Kitt Peak 12-m telescope, which we combined with the H I rotation curve. The CO rotation observed for the inner $5'$ region agrees with the H I rotation. The rotation velocity increases steeply near the nucleus, but reaches only to 20 km s^{-1}, and turns to increase more gently from the inner $1'$ region to $10'$. It continues to increase monotonically to the observed edge at $30'$. This galaxy shows neither a steep rise nor a sharp central peak, similarly to NGC 4631, and is exceptional among the galaxies studied here. Note that both M33 and NGC 4631 are low-mass galaxies.

NGC 660: This is a nearly edge-on Sc galaxy with a polar ring (van Driel et al. 1995). We applied the envelope-tracing method to the H I position–velocity diagrams for the disk and polar ring, as well as to the CO(2–1) position velocity diagram for the inner part. The rotation curve of the disk can be apparently connected smoothly to that of the polar ring. Since the polar-ring rotation will manifest

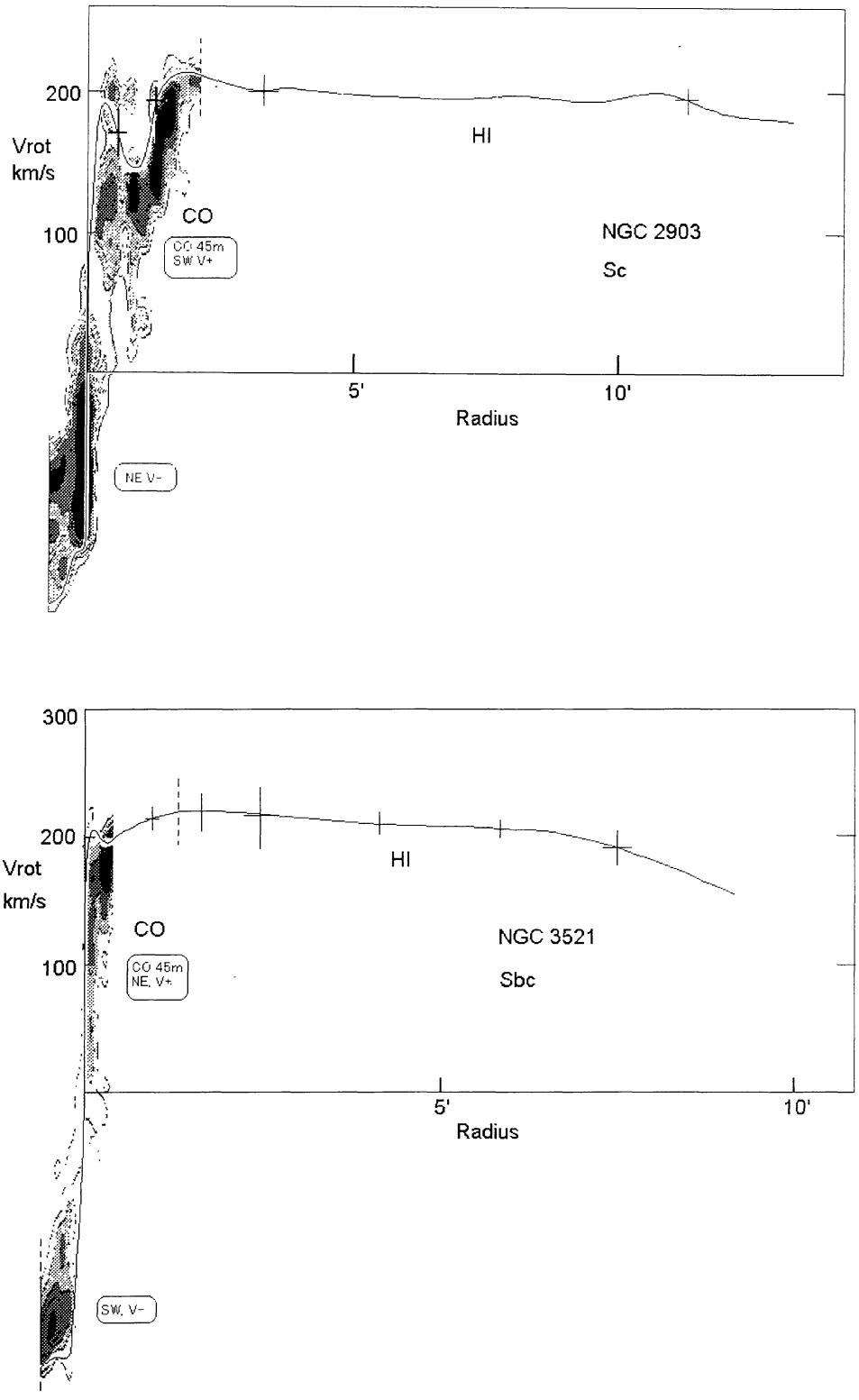

Fig. 1. Examples of position–velocity diagrams in the CO line emission for some galaxies, and traced rotation curves, which are smoothly connected with H I rotation curves. Crosses indicate typical errors (vertical) and angular resolution (horizontal).

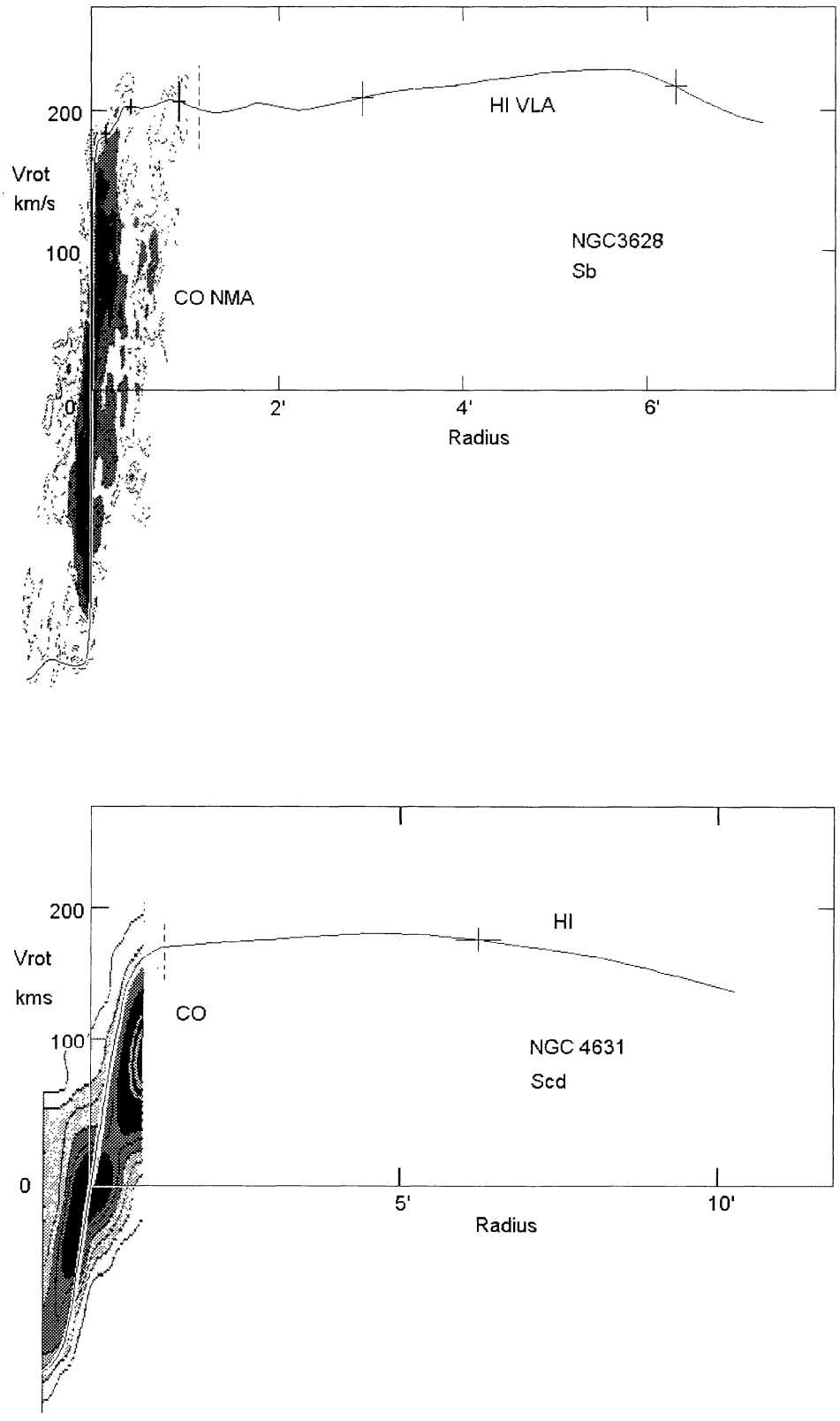

Fig. 1. (Continued)

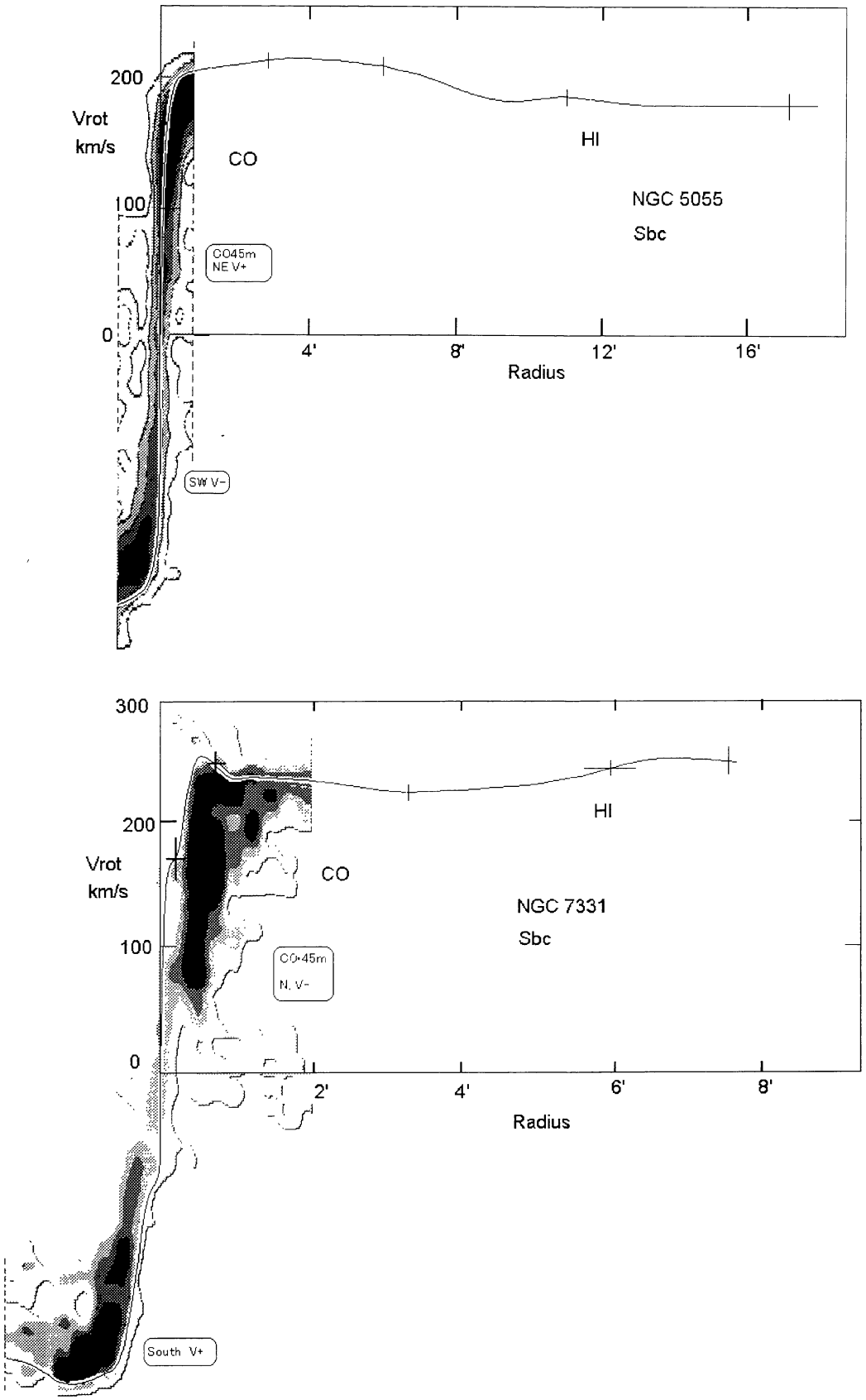

Fig. 1. (Continued)

Table 1. Parameters for galaxies and references for PV diagrams and rotation curves.

Galaxy	Type	Inclination (°)	Distance* (Mpc)	Line	Telescope†	Angular resolution (″)	References
NGC 224 (M31)	Sb	77	0.69	Opt [N II]			Rubin, Ford 1970
				Hα			Ciardullo et al. 1988
				H I	E100m	540	Cram et al. 1980
NGC 253	Sc	78.5	2.5	...	...	...	Paper I
				CO	N45m	15	Nishiyama 1995
IC 342	Sc	25	3.9	...	...	...	Paper I
NGC 598 (M33)	Sc	54		H I	CI	47	Newton 1980
			0.79	CO	K12m	55	Wilson, Scoville 1989
NGC 660	Sc	70	13	H I	W	20	van Driel et al. 1995
Polar ring				H I	W	60	ibid
				CO 2–1	I30m	12	ibid
NGC 891	Sb	88.3	8.9	...	...	...	Paper I
NGC 1068	Sb Sy	46	18.1	Opt			Kaneko et al. 1992b
				Opt			Galleta, Recillas-Cruz 1982
				CO	N45m	17	Kaneko et al. 1989
				CO	NMA	5 × 4	Kaneko et al. 1992a
NGC 1097	SBb	40	16	CO	N45m	15	Gerin et al. 1988
				H I	V	25	Ondrechen et al. 1989
NGC 1365	SBb	46	15.6	H I	V	36 × 23	Ondrechen, van der Hulst 1989
				CO 2–1	S15m	25	Sandqvist et al. 1995
NGC 1808	Sbc	58	11.4	...	...	...	Paper I
NGC 2403	Sc	60	3.25	H I	W	40/60	Lake, Feinswog 1989
				CO	K12m	60	Thornley, Wilson 1995
NGC 2841	Sb	68	9	H I	W	51 × 65	Bosma 1981a
				CO	F14m	45	Young et al. 1995
NGC 2903	Sc	35	6.1	H I	W		Lake, Feinswog 1989
				CO	N45m	15	Sofue et al. (in preparation)
NGC 3031 (M81)	Sb	59	3.25	Opt			Goad 1976
				CO	K12m	55	Sage, Westpfahl 1991
				H I	W	25/50	Rots 1975
NGC 3034 (M82)	Ir	80–90	3.25	CO 2–1	I30m	13	Sofue et al. 1992
				H I	V	18	Yun et al. 1993
NGC 3079	Sc	∼90	15.6	...	...	...	Paper I
NGC 3198	SBc	70	9.1	H I	W	25 × 35	Bosma 1981a
				H I	W	25 × 35	Begeman 1989
				Opt			Hunter et al. 1986
NGC 3521	Sbc	75	8.9	H I	W	74 × 53	Casertano, van Gorkom 1991
				CO	N45m	15	Sofue et al. (in preparation)
NGC 3628	Sb(Ir)	>86	6.7	CO	NMA	3.9	Irwin, Sofue 1995
				H I	V	15	Wilding et al. 1993

the gravitational potential in the halo, which is supposed to be round, we may approximate the outer rotation curve in the disk plane by this polar ring curve. The CO line profiles indicate that the maximum rotation velocity occurs near the center, in an unresolved region of $< 10''$. The inner CO rotation has a high central peak of about 190 km s^{-1}, followed by a disk rotation, where H I and CO velocities coincide well.

NGC 891: This edge-on galaxy has been studied extensively using the PV diagrams in the CO and H I emissions. The rotation curve is similar to that of the Milky Way, showing a nuclear rise and peak followed by a flat disk rotation and a declining outer part. See Paper I for the detail and for references.

NGC 1068: This is a Seyfert galaxy. The position angle of the major axis is not well defined. We adopted 70° for the outer and disk region as read from the outer optical velocity field as well as from the optical image,

Table 1. (Continued)

Galaxy	Type	Inclination (°)	Distance* (Mpc)	Line	Telescope†	Angular resolution (″)	References
NGC 4258	Sbc	67	6.6	H I	W	40	van Albada, Shane 1976
				CO	N45m	15	Sofue et al. 1989a
NGC 4303	Sc	27	8.1	CO	N45m	15	Nishiyama 1995
				CO	NMA	4	Sofue et al. (in preparation)
				H I	V	45	Guhathakurta et al. 1988
NGC 4321 (M100)	Sc	27	15	CO	N45m	15	Nishiyama 1995
				CO	NMA	4	Sakamoto 1995
				H I	V		Knapen et al. 1993, 1995
NGC 4565	Sb	86	10.2	...	...	...	Paper I
NGC 4569	Sab	63	8.2	CO	N45m	15	Nishiyama 1995
				CO	NMA	9.9 × 4.8	Sofue et al. (in preparation)
				H I	V	20	Guhathakurta et al. 1988
NGC 4631	Sc Ir	84	5.2	H I	W	48 × 89	Weliachev et al. 1978
				CO	N45m	15	Sofue et al. 1989b, 1997
				CO(2–1)	I30m	13	Sofue et al. 1990
NGC 4736	Sab	35	5.1	CO	N45m	15	Nishiyama 1995
				H I	W	25 × 38	Bosma et al. 1977
NGC 4945	Sc I	78	6.7	CO(2–1)	S15m	24	Dahlem et al. 1993
				CO(1–0)	S15m	43	ibid
				H I	TE		Ables et al. 1987
NGC 5033	Sc	62	14	CO	N45m	15	Nishiyama 1995
				H I	W	51 × 85	Bosma 1981a
NGC 5055	Sbc	55	8	H I	W	49 × 73	Bosma 1981a
				CO	N45m	15	Sofue et al. (in preparation)
NGC 5194 (M51)	Sc	20	9.6	...	...	...	Paper I
NGC 5236 (M83)	SBc	24	8.9	CO	N45m	15	Handa et al. 1990; Nishiyama 1995
				H I	W	40	Bosma et al. 1981
NGC 5457 (M101)	Sc	18	7.2	H I	W	24 × 30	Bosma et al. 1981
				CO	F14m	50	Kenney et al. 1991
NGC 5907	Sc	88	11.6	...	...	...	Paper I
NGC 6946	Sc	30	5.5	...	...	...	Paper I
NGC 6951	Sbc	48		CO	N45m	15	Nishiyama 1995
				Opt			Marquez, Moles 1993
NGC 7331	Sbc	75	14	H I	W	25 × 45	Bosma 1981a
				CO	N45m	15	Sofue et al. (in preparation)
Milky Way (outside solar circle)	Sb	90	0	CO+H I			Clemens 1995
				H I			Honma, Sofue 1996a,b

* Distances have been taken from the references in the same row. For the original data, refer to the literature.

† (CO-line observations) N45m = NRO 45-m telescope; I30m = IRAM 30-m telescope; S15m = SEST 15m telescope; F14m = FCRAO 14-m telescope; K12m = NRAO Kitt-Peak 12-m telescope; NMA = Nobeyama Millimeter Array. (H I-line observations) E100m = Effelsberg 100-m telescope; CI = Cambridge Interferometer; W = WSRT; V = VLA; TE = Two- Element Synthesis telescope. (Optical observations) Opt = Optical line (e.g., Hα) observations.

and 90° for the central region from the CO velocity field (see the literature cited in table 1). The rotation velocity appears to rise steeply in the center toward the peak on the molecular ring. However, the very central behavior is not observed due to the lack of CO emission at the center.

NGC 1097: If the adopted inclination angle of 40° is correct, the apparent rotation velocity of the molecular ring is as high as 350 km s^{-1}, showing a nuclear peak. The rotation decreases, then dips at 40″ radius, followed by a broad maximum of about 300 km s^{-1} at 2′; it then flattens and slowly declines toward the edge. The general characteristic is similar to that of the Milky Way, except for the velocity amplitude.

NGC 1365: This is a typical barred spiral with a Seyfert nucleus. The CO data from the SEST 15-m telescope indicate a steep rise and a central peak at 240 km s^{-1}, followed by a disk component as high as 270 km s^{-1}, and then a monotonically declining rotation observed in the H I line.

NGC 1808: A steep nuclear rise and a peak are followed by a gradual decrease toward the edge of the observed rotation curve. See Paper I.

NGC 2403: Due to its proximity, we used the lower-resolution CO data from the Kitt Peak 12-m telescope. No higher-resolution observations are available. The RC increases steeply in the center until 80 km s^{-1}, then increases slowly until 5′ radius, where the curve turns to be flat at a velocity as low as 120 km s^{-1}. The CO and H I curves agree with each other at 1′ to 5′, while the CO velocity is much higher in the central 1′ region.

NGC 2841: Since no high-resolution CO data are available, we used the FCRAO 14m CO data for the inner 4′ to derive a CO rotation curve, and combined it with the outer H I rotation curve. Although the very central kinematics is not clear, due to the weak CO emission near the nucleus, a steep rise within the central 1′ region and a peak as high as 310 km $s^{-1}$are visible. After increasing to a maximum of 330 km s^{-1} at 2′ to 3′, the velocity decreases and turns to be flat at 270 km s^{-1}until the edge.

NGC 2903: The CO rotation curve has a peculiar step at 1′–2′ radius with a maximum of about 170 km s^{-1} at 1′. It, then, increases to a second maximum of 200 km s^{-1} at 3′. The step is, however, asymmetric with respect to the center. This inner maximum has a higher velocity in the SW side than in the NE. The outer rotation from H I, however, is very flat until the edge.

NGC 3031 (M81): Optical and CO-line data have been combined for the central 2′. The rotation has a central peak at 300 km s^{-1}, although the peak is not very sharp. The H I rotation from the disk to outer region is similar to that of the Milky Way in shape and velocity.

NGC 3034 (M82): This is an interacting peculiar galaxy with a starburst activity and is rich in CO gas. The CO (J = 2–1) data obtained by the IRAM 30-m telescope show a clearly declining rotation curve, well fitted by Keplerian rotation. The VLA H I data agree with the CO data, though the error is larger.

NGC 3079: A sharp and high-velocity nuclear rise and a peak, and then a gap, are followed by a disk component, similar to that of the Milky Way. The outer rotation is declining. See Paper I.

NGC 3198: The central steep rise stops at a peak as low as 50 km s^{-1}. Then, the rotation increases in a rigid-body fashion, showing a next step. The disk part has a broad maximum of 170 km s^{-1}, followed by a flat rotation.

NGC 3521: The inner rotation curve increases steeply, and attains a small and sharp central peak at 10″ of 210 km s^{-1}, followed by a dip at 20″. It then increases slowly until a broad maximum at 1.′5. The outer H I RC gradually decreases until the edge.

NGC 3628: The CO PV diagram, as obtained by interferometer observations with the Nobeyama Millimeter Array, shows a nuclear disk asymmetric with respect to the position–velocity center of the outer disk. We took the center of the nuclear disk as the origin of the rotation curve, and connected the inner RC with the outer rotation curve by averaging the position and velocities in both sides of the nucleus. The CO+H I RC has a steep rise near to the center within 5″, indicating a nuclear disk, rotating at 190 km s^{-1}. It further increases to 200 km s^{-1} at 1′, and is followed by a flat rotation in the outer disk.

NGC 4258: The velocity increases to a maximum of 230 km s^{-1} within the central 30″, and decreases to a flat part at 3′ to 7′. The outer H I rotation is almost flat after a broad maximum at 10′ radius.

NGC 4303: The rotation curve for the central 15″ has been derived using a position–velocity diagram at a constant declination obtained by the NMA. The correction for position-angle and inclination resulted in a high-velocity peak, which is not clearly seen in the 45-m data. The error for the central peak is, therefore, as large as $\sim$ 30 km s^{-1}. The disk and outer parts of the rotation curve are flat.

NGC 4321 (M100): The NMA observation shows a steeply increasing rotation within a 5″ radius to a central peak of 230 km s^{-1} at 10″, followed by a dip at 20″. The RC thus gradually increases until 3′ to a broad maximum of 270 km s^{-1} in H I velocity. The outermost rotation velocity is not certain because of the warped H I disk and low inclination.

NGC 4565: This is a typical edge-on galaxy of Sc type. The rotation has a central peak and a flat disk-to-outer rotation. It shows an indication of declining in the outermost region. See Paper I.

NGC 4569: This is Virgo galaxy which shows a truncated H I gas disk. CO-line position–velocity diagrams obtained with the NMA at a 9″ resolution show a sharp rise to a 200 km s^{-1} central peak. The 45-m data show a rotation minimum at 40″, followed by an increase toward the H I high-velocity rotation in the outer disk. The outskirts of H I gas are missing, possibly due to ram-pressure stripping by the intra-cluster gas.

NGC 4631: This is an interacting, edge-on semi-dwarf galaxy. The CO RC in the central 40″ is rigid-body like, having neither a nuclear rise nor a peak. The RC is followed by a flat and declining H I rotation in the outer disk. This galaxy is one of the two exceptions (with M33), which show no nuclear rise of rotation in CO. However, the intensity distribution along the major axis indicates no concentration of CO gas in the center, but

either a ring or clumps avoiding the nucleus (Sofue et al. 1989). Therefore, the apparent rigid-body rotation in the position–velocity diagram may be due to the lack of gas near the nucleus, even if the true rotation curve has a sharper rise.

NGC 4736: The rotation rises steeply within 12″, and attains a central peak at 18″. It then decreases monotonically toward the observed edge.

NGC 4945: We used position–velocity diagrams along the major axis from the two-elements interferometric observations to derive an H I rotation curve, and those from the SEST 15-m observations in the CO (J = 1–0) and CO (J = 2–1) emissions. We adopted the higher-resolution CO (2–1) data for the inner region, CO (1–0) for the disk, and H I for the outer region. They agree in the overlapped regions, except that the CO (2–1) data indicate a sharper central peak of RC than CO (1–0). The obtained RC is similar to that of our Galaxy. It has a steep rise and a sharp central peak, followed by a broad maximum in the disk and a flat part in the outskirts.

NGC 5033: A sharp rise to a central peak at 10″ is followed by a second peak at 35″. The outer H I rotation is flat until the edge, indicating declining rotation near the edge.

NGC 5055: A sharp, rigid body-like rise within the central 30″ is followed by a flat part till a broad maximum at 4′. The rotation declines then until 8′, beyond which it is nearly flat.

NGC 5194 (M51): A steep rise in the center is followed by a flat disk rotation until 2.′7 radius, superposed by high-amplitude velocity deviation due to the spiral arms. The rotation velocity then declines more rapidly than a Keplerian curve. This may be due to the gravitational disturbance by the companion NGC 5195, or to a warp in the outer disk likely caused by the tidal interaction. See Paper I.

NGC 5236 (M83): The RC rises very steeply near the center, attaining a sharp peak at 10″ of 250 km s^{-1}. It then decreases steeply toward a deep dip at 30″ with a minimum velocity as low as 120 km s^{-1}. The RC again increases toward a second broad maximum at 2′ of 190 km s^{-1}, and is followed by a gradually declining H I part in the outer disk. The sharp central peak and deep dip are peculiar among the galaxies so far known of the rotation curves, and may be related to the bar and accretion process.

NGC 5457 (M101): This is a nearly face-on Sc galaxy, but no high-resolution CO data are available. Because of its large apparent size, we used lower-resolution CO data from the Kitt Peak 12-m telescope. The central rise within the beam width 30″ is recognized, but the resolution is not sufficient for discussing the detail about the nuclear rise.

NGC 5907: This is an almost perfectly edge-on galaxy. The central RC rises steeply to a shoulder of 200 km s^{-1} at 10″. The RC further continues to increase until 4′ radius, and then declines toward the edge. See Paper I.

NGC 6946: The central peak is very sharp, and as high as 240 km s^{-1}, followed by a gap which is rather flat until the second increase toward the disk maximum starts. This rotation curve is similar to that of the Milky Way. See Paper I.

NGC 6951: The central high-velocity peak of 260 km s^{-1} is remarkable at a radius of 20″. Since the resolution of the 45-m telescope is not enough to resolve this region due to the relatively large distance, the true peak velocity may be much higher. The CO RC has been combined with the Hα data for the disk part, showing a gradually increasing toward the outer region.

NGC 7331: The central steep rise has a shoulder-like step of 130 km s^{-1} at 14″, and reaches a peak of 240 km s^{-1} at 34″ after a rigid-body like increase. The outer H I rotation is almost flat, slightly increasing until the end of the disk.

Milky Way: For a comparison, we show the rotation curve for our Galaxy. The Sun's distance from the nucleus is taken to be 8 kpc. The RC within the solar circle was taken from Clemens (1995), and that for the outer region from Honma and Sofue (1996a, b). See the literature for details.

4. Discussion

4.1. Steep Nuclear Rise

We have derived the CO rotation curves of the central regions for nearby spiral galaxies, and combined them with outer H I rotation curves. A remarkable feature obtained in the present study is the steep nuclear rise of rotation within a radius smaller than the beam width of CO observations. Two exceptional cases were found: A nearby Sc galaxy, M33, known for its low surface brightness, shows a rapid rise in the center, but to a low velocity, and then a gentle rise; NGC 4631, a semi-dwarf edge-on galaxy of amorphous type, has a rigid-body rise. However, NGC 4631's case might be an apparent phenomenon due to the lack of CO gas near the center, and the true rotation curve may have a sharper rise. Hence, the only one exception indeed having a slowly rising rotation is M33.

4.2. The Nuclear Mass Component

In Paper I we have shown that the steeply rising rotation curves can be generally fitted by a model with four mass components: the nuclear compact mass, central bulge, disk, and the massive halo. Particularly, such a steep rise within the central few hundred parsecs as observed for NGC 3079, NGC 4321, and NGC

6946 by high-resolution interferometer observations indicates the existence of a compact nuclear mass of a 100 to 150 pc radius and a mass of several 10^9 $M_\odot$. Hence, some of the galaxies are likely to be nested by a more compact stellar mass concentration in the center than the usual bulges, which we called a bulge-in-bulge.

In order to avoid the discontinuity of envelope-traced terminal velocities from both sides of the nucleus on the position–velocity diagrams, we have connected them by a solid-body like line crossing the nucleus at zero velocity within a radius comparable to the angular resolution. Therefore, the curves drawn within regions smaller than the angular resolution may not represent the true velocities. It is more likely that the true rotation curve has a sharper, unresolved rise. It is also likely that the velocity remains finite until the nucleus, or even increases, since the galactic nuclei are often nested by a compact massive object.

4.3. Circular Rotation-vs-Bar Debate

By definition, a rotation curve is the trace of terminal velocities in the position–velocity diagram along the major axis. It may be superposed by non-circular motions, such as that due to the density waves, bars and oval potential, or interaction with the companion. It is, therefore, not straightforward to derive the mass distribution using the curves by assuming a circular rotation. Nevertheless, this assumption has been extensively adopted in deriving the mass of galaxies, including hypothetical dark halos. The mass and potential derived from the circular-rotation assumption have also been used to discuss the inner and outer Lindblad resonances, or to analyze the pattern speed and density waves. Rotation curves have also been used to derive the mass distributions in the bulges and central cores, and have shown good agreement with the surface photometry (e.g., Kent 1987). These studies have made available the most important parameters of the galaxies, and the circular-rotation assumption appears to be reasonable in so far as the basic structures of galaxies are analyzed.

On the other hand, it is a trend to introduce a bar in the analysis. However, if one stands on a bar hypothesis, the so-called rotation curves will give no additional quantitative information about the mass, unless the true potential is determined by independent observations. One might argue that the nuclear rise and peak of rotation may be due to a high-velocity flow of gas along a bar parallel to the line of sight, whereas the mass (potential) distribution is not known, which is necessary to calculate the flow. However, the probability of looking at a bar from its end is far smaller compared to that of looking at it at a finite angle. In the latter case, the gas along the bar will be observed roughly at the bar's pattern speed, and, therefore, will show a rigid-body like rotation at lower velocities than a circular rotation. Hence, if some cases of the nuclear rise of rotation are due to a bar indeed, a larger number of galaxies must be observed to show a gentle rise in a rigid-body fashion. This, however, is not the case at all. Note that M33 has no bar, and NGC 4631 is an amorphous dwarf and does not provide a firm case for rigid body rotation. Hence, it is not likely that the nuclear rise observed in almost all galaxies studied here is due to a bar-induced gas flow.

We may, therefore, reasonably assume that the central rotation is circular in the zero-th order approximation, and the observed rotation curves manifest the mass distribution within the bulges. This can be clarified by comparing the observed rotation curves with those calculated by a mass model based on a surface photometry assuming an appropriate mass-to-light ratio, as has been obtained for disk regions by Kent (1987) on the basis of optical data. Since the nuclear region is highly obscured in optical wavelengths, we may need infrared surface photometry for a comparison, which will be described in a separate paper.

References

Ables J.G., Forester J.R., Manchester R.N., Rayner P.T., Whiteoak J.B., Mathewson D.S., Kalnajs A.J., Peters W.L., Wehner H. 1987, MNRAS 226, 157

Begeman K.G. 1989, A&A 223, 47

Bosma A. 1981a, AJ 86, 1791

Bosma A. 1981b, AJ 86, 1825

Bosma A., Goss W.M., Allen R.J. 1981, A&S 93, 106

Bosma A., van der Hulst J.M., Sullivan W.T. III 1977, A&A 57, 373

Casertano S. 1983, MNRAS 203, 735

Casertano S., van Gorkom J.H. 1991, AJ 101, 1231

Ciardullo R., Rubin V.C., Jacoby G.H., Ford H.C., Ford W.K. Jr 1988, AJ 95, 438

Clemens D.P. 1985, ApJ 295, 422

Combes F. 1992, ARA&A 29, 195

Combes F., Gottesman S.T., Weliachew L. 1977, A&A 59, 181

Cram T.R., Roberts M.S., Whitehurst R.N. 1980, A&AS 40, 215

Dahlem M., Golla G., Whiteoak J.B., Wielebinski R., Hüttemessiter S., Henkel C. 1993, A&A 270, 29

Galletta G., Recillas-Cruz E. 1982, A&A 112, 361

Gerin M., N., Combes F. 1988, A&A 203, 44

Goad J.W. 1976, ApJS 32, 89

Guhathakurta P., van Gorkom J.H., Kotanyi C.G., Balkowski C. 1988, AJ 96, 851

Handa T., Nakai N., Sofue Y., Hayashi M., Fujimoto M. 1990, PASJ 42, 1

Honma M., Sofue Y. 1996a, PASJ submitted

Honma M., Sofue Y. 1996b, PASJ 48, L103

Hunter D.A., Rubin V.C., Gallagher J.S. III 1986, AJ 91, 1086

Irwin J.A., Sofue Y. 1996, ApJ 464, 738

Kaneko N., Morita K., Fukui Y., Sugitani K., Iwata T., Nakai N., Kaifu N., Liszt H. 1989, ApJ 337, 691
Kaneko N., Morita K., Fukui Y., Takahashi N., Sugitani K., Nakai N., Morita K. 1992a, PASJ 44, 341
Kaneko N., Satoh T., Toyama K., Sasaki M., Nishimura M., Yamamoto M. 1992b, AJ 103, 422
Kenney J.D.P., Scoville N.Z., Wilson C.D. 1991, ApJ 366, 432
Kenney J., Young S.J. 1988, ApJS 66, 261
Kent S.M. 1987, AJ 93, 816
Knapen J.H., Beckman F.E., Heller C.H., Sholosman I., de Jong R.S. 1995, ApJ 454, 623
Knapen J.H., Cepa J., Beckman J.E., Soledad del Rio M., Pedlar A. 1993, ApJ 416, 563
Lake G., Feinswog L. 1989, AJ 98, 166
Marguez I., Moles M. 1993, AJ 105, 2050
Newton K. 1980, MNRAS 190, 689
Nishiyama K. 1995 Ph.D. Thesis, The University of Tokyo
Ondrechen M.P., van der Hulst J.M. 1989, ApJ 342, 29
Ondrechen M.P., van der Hulst J.M., Hummel E. 1989, ApJ 342, 39
Persic S., Salucci P., Stel F. 1996, MNRAS 281, 27
Planesas P., Scoville N., Myers S.T. 1991, ApJ 369, 364
Rots A.H. 1975, A&A 45, 43
Rubin V.C., Ford W.K. Jr 1970, ApJ 159, 381
Rubin V.C., Ford W.K., Thonnard N. 1980, ApJ 238, 471
Rubin V.C., Ford W.K., Thonnard N. 1982, ApJ 261, 439
Sage L.I., Westpfahl D.J. 1991, A&A 242, 371
Sakamoto K. 1995, Ph.D. Thesis, The University of Tokyo
Sakamoto K., Okumura S., Minezaki T., Kobayashi Y., Wada K. 1995, AJ 110, 2075
Sandqvist Aa., Jörsäster S., Lindblad P.O. 1995, A&A 295, 585
Sofue Y. 1996, ApJ 458, 120 (Paper I)
Sofue Y., Doi M., Krause M., Nakai N., Handa T. 1989a, PASJ 41, 113
Sofue Y., Handa T., Golla G., Krause M., Wielebinski R. 1990, PASJ 42, 745
Sofue Y., Handa T., Nakai N. 1989b, PASJ 41, 937
Sofue Y., Honma M., Arimoto N. 1994, A&A 296, 33
Sofue Y., Kato R. 1981, PASJ 33, 449
Sofue Y., Reuter H.-P., Krause M., Wielebinski R., Nakai N. 1992, ApJ 395, L126
Sofue Y., Yoshida Y. 1993, ApJ 417, L63
Thornley M.D., Wilson C.D. 1995, ApJ 447, 616
van Albada G.D., Shane W.W. 1976, A&A 42, 433
van Driel W., Combes F., Casoli F., Gerin M., Nakai N., Miyaji T., Hamabe M., Sofue Y. 1995, AJ 109, 942
Weliachev L., Sancisi R., Guélin M. 1978, A&A 65, 37
Wilding T., Alexer P., Green D.A. 1993, MNRAS 263, 1075
Wilson C.D., Scoville N. 1989, ApJ 347, 743
Young J.S., Scoville N.Z. 1992, ARA&A 29, 581
Young J.S., Xie S., Tacconi L., Knezek P., Vicuso P., Tacconi-Garman L., Scoville N., Schneider S. et al. 1995, ApJS 98, 219
Yun M.S., Ho P.T.P., Lo K.Y. 1993, ApJ 411, L17

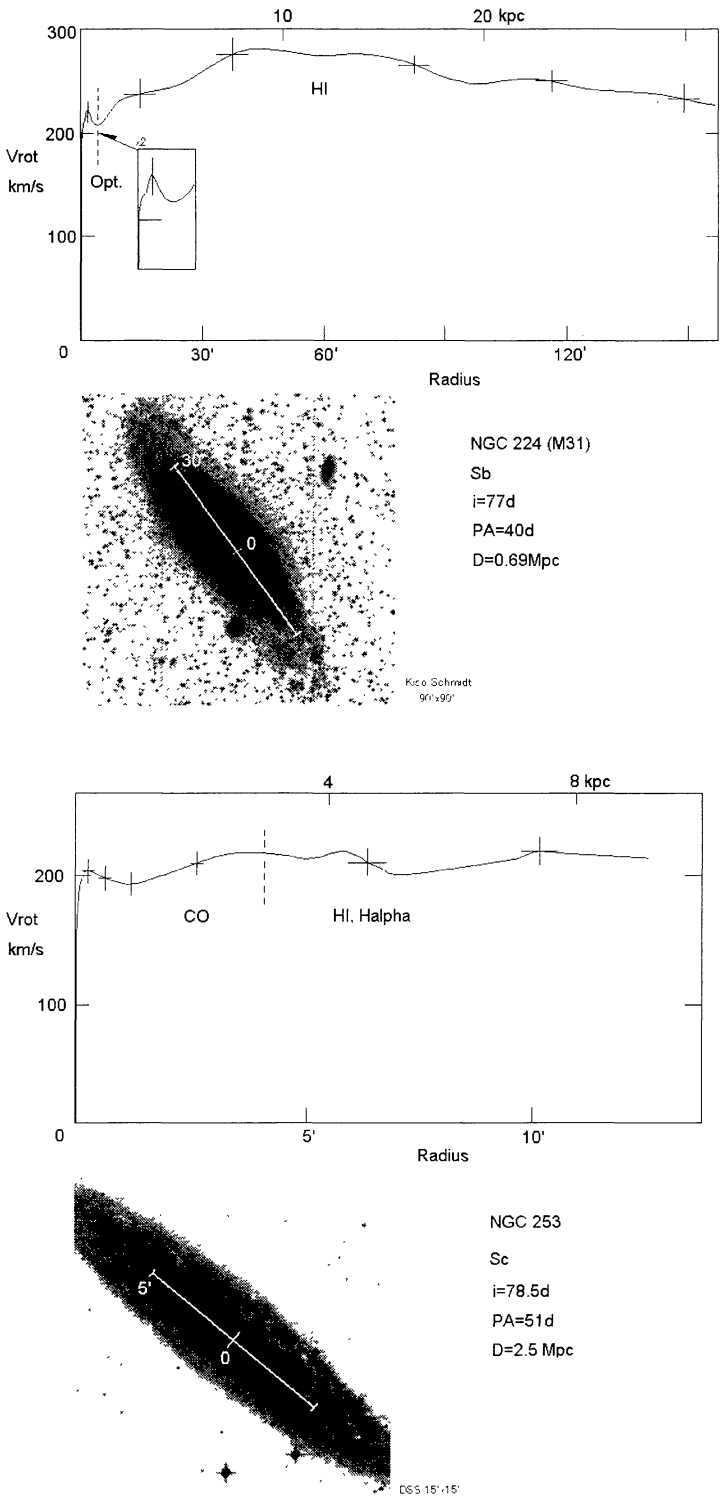

Fig. 2. Inner-to-out rotation curves obtained by combining CO and H I rotation curves of galaxies. Some curves have been obtained by using optical data. Typical angular resolutions and errors are indicated by crosses at several representative points for each object. The horizontal bars indicate the angular resolutions, and the vertical bars give errors in the rotation velocity estimates. The dashed vertical lines indicate the borders of CO and H I rotation curves. The borders of regions with different data of different angular resolutions are also indicated by dashed lines. Optical images from the STScI Digitized Sky Survey are shown with the major axes and angular scales superposed.

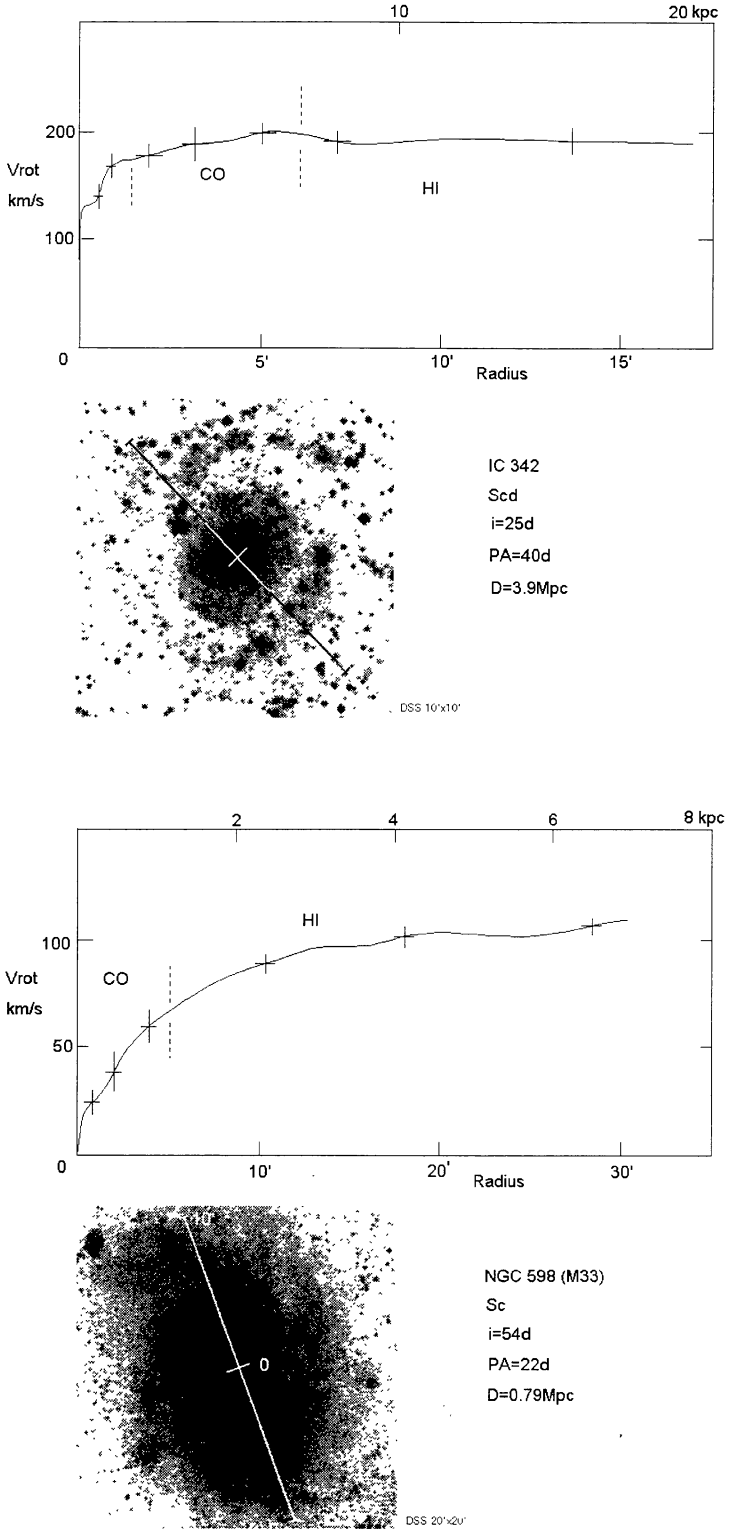

Fig. 2. (Continued)

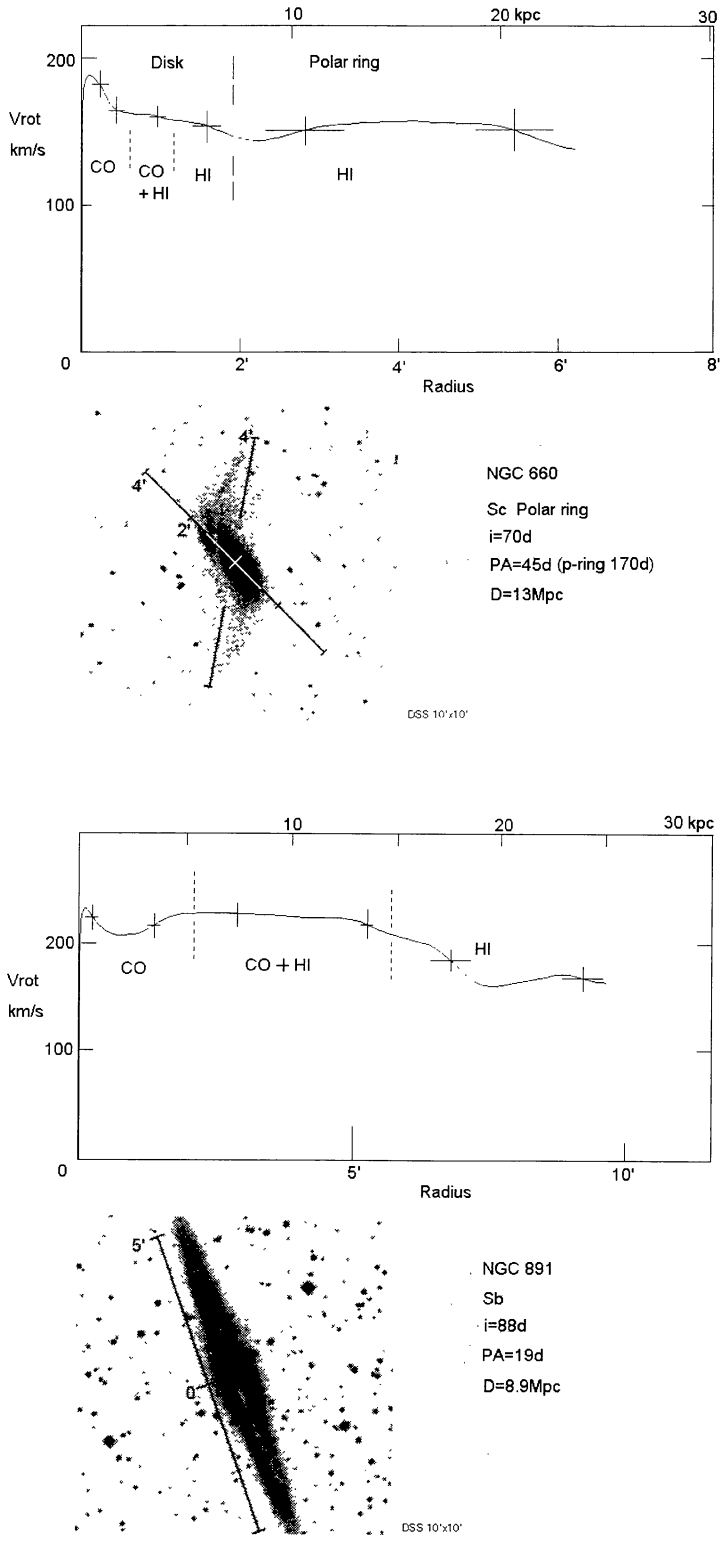

Fig. 2. (Continued)

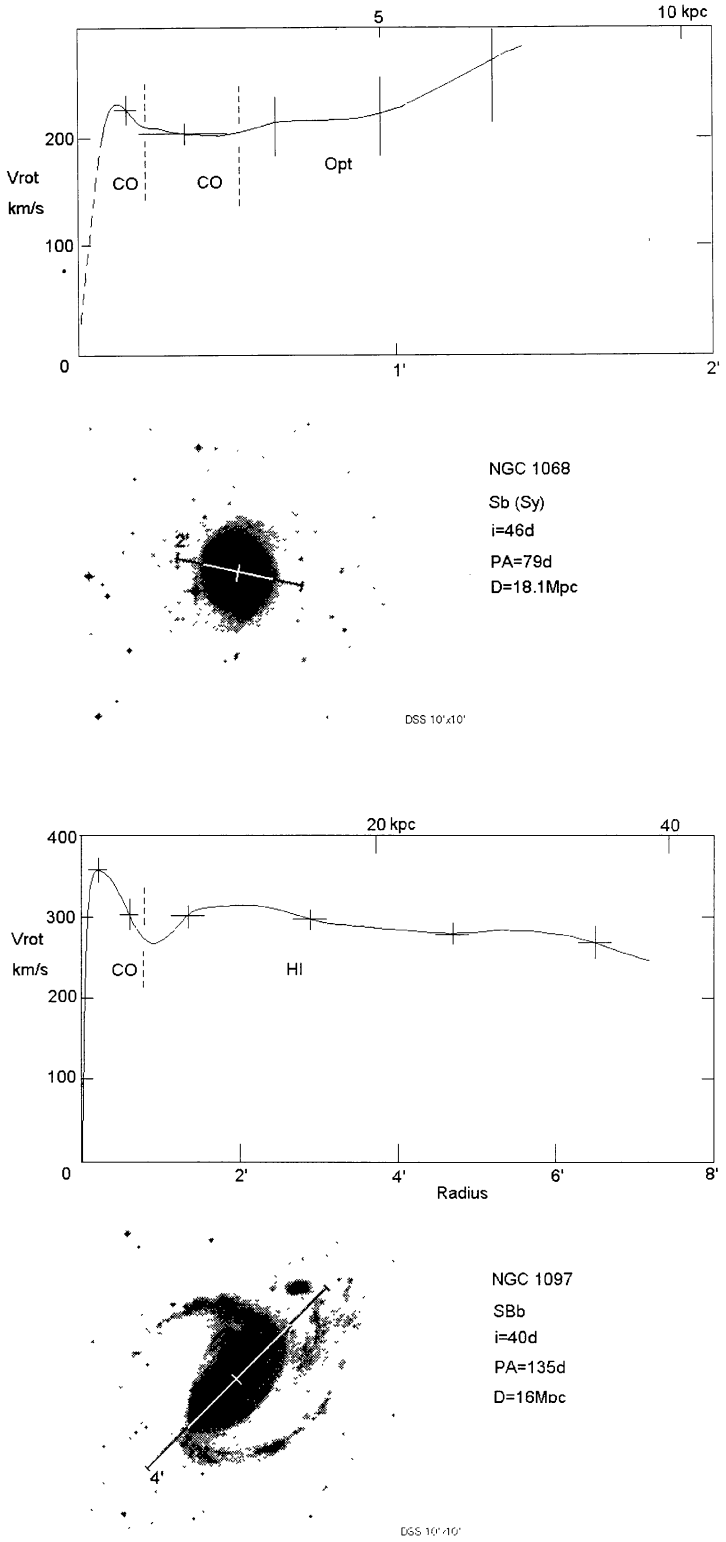

Fig. 2. (Continued)

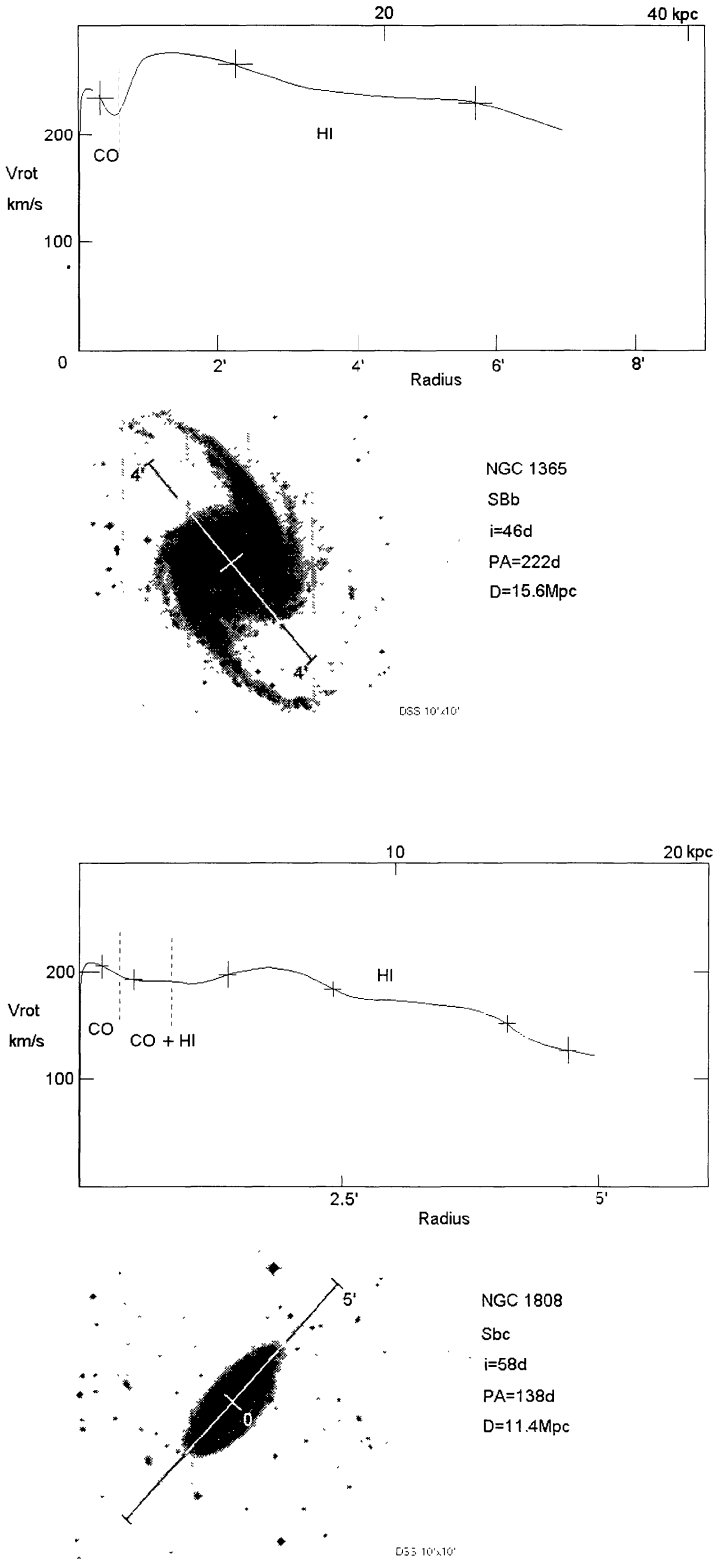

Fig. 2. (Continued)

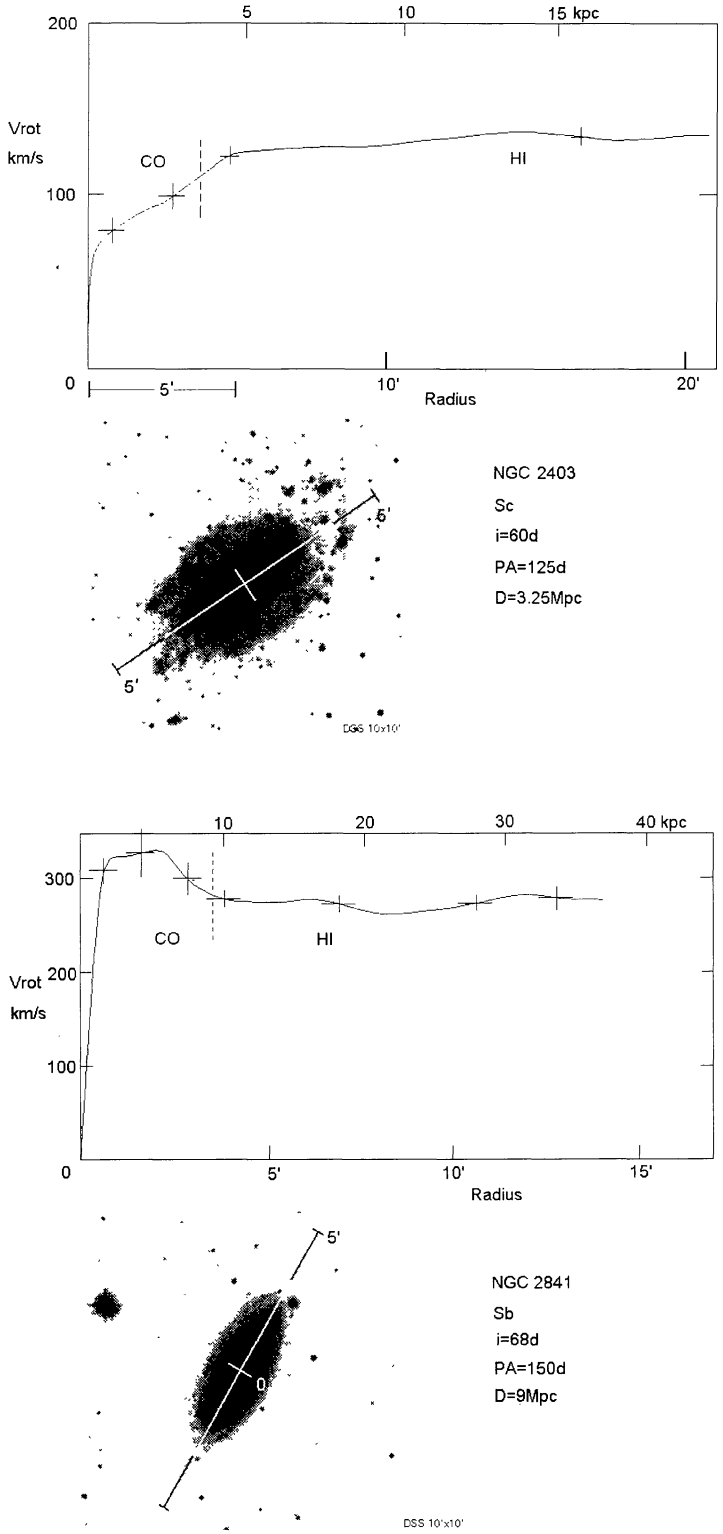

Fig. 2. (Continued)

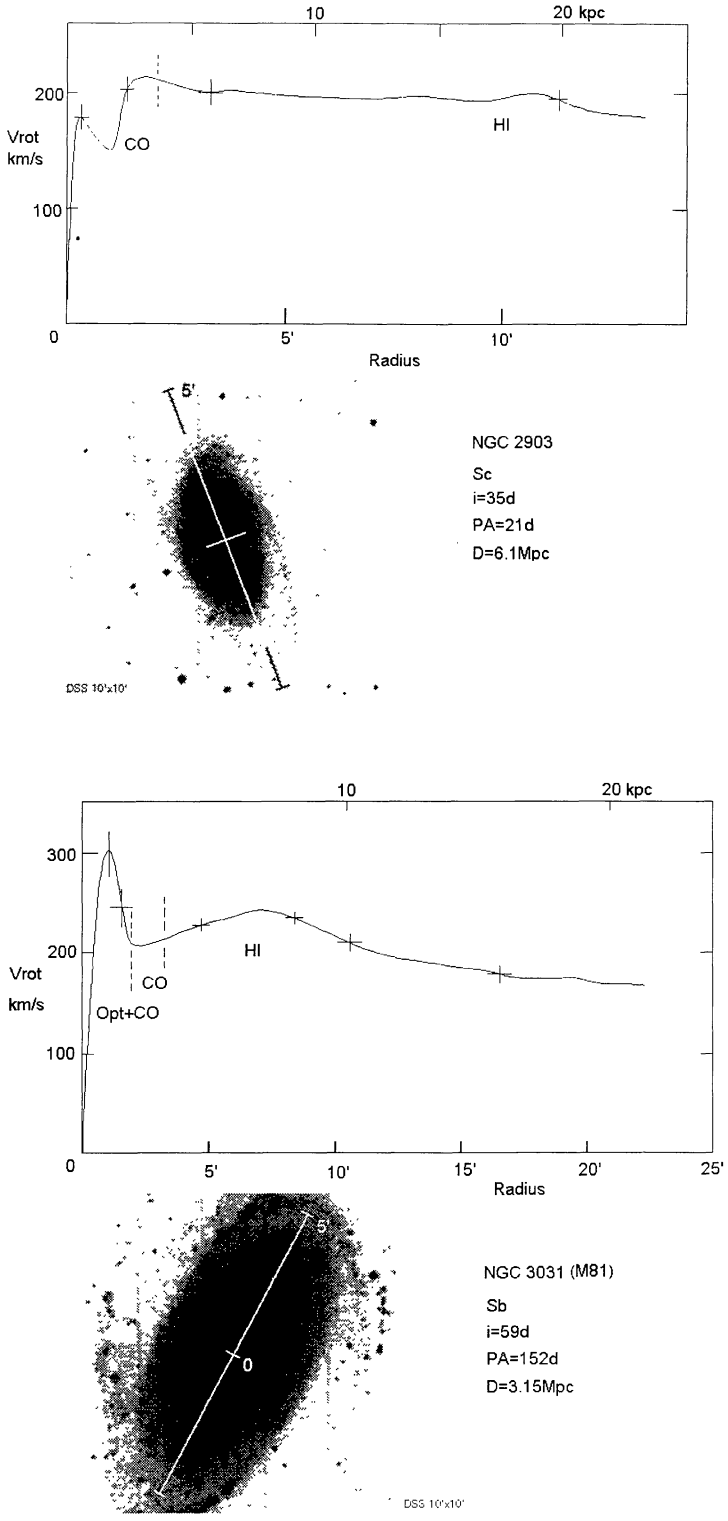

Fig. 2. (Continued)

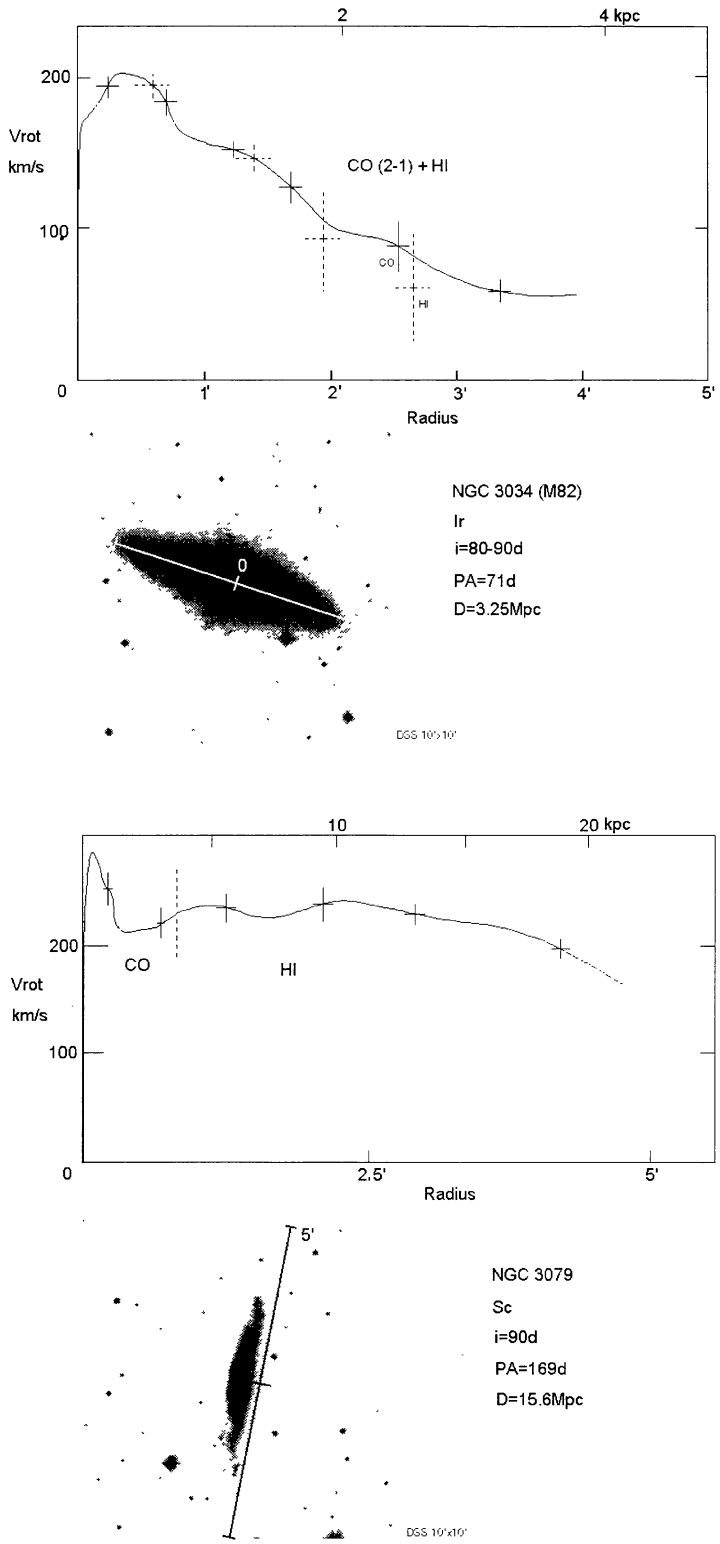

Fig. 2. (Continued)

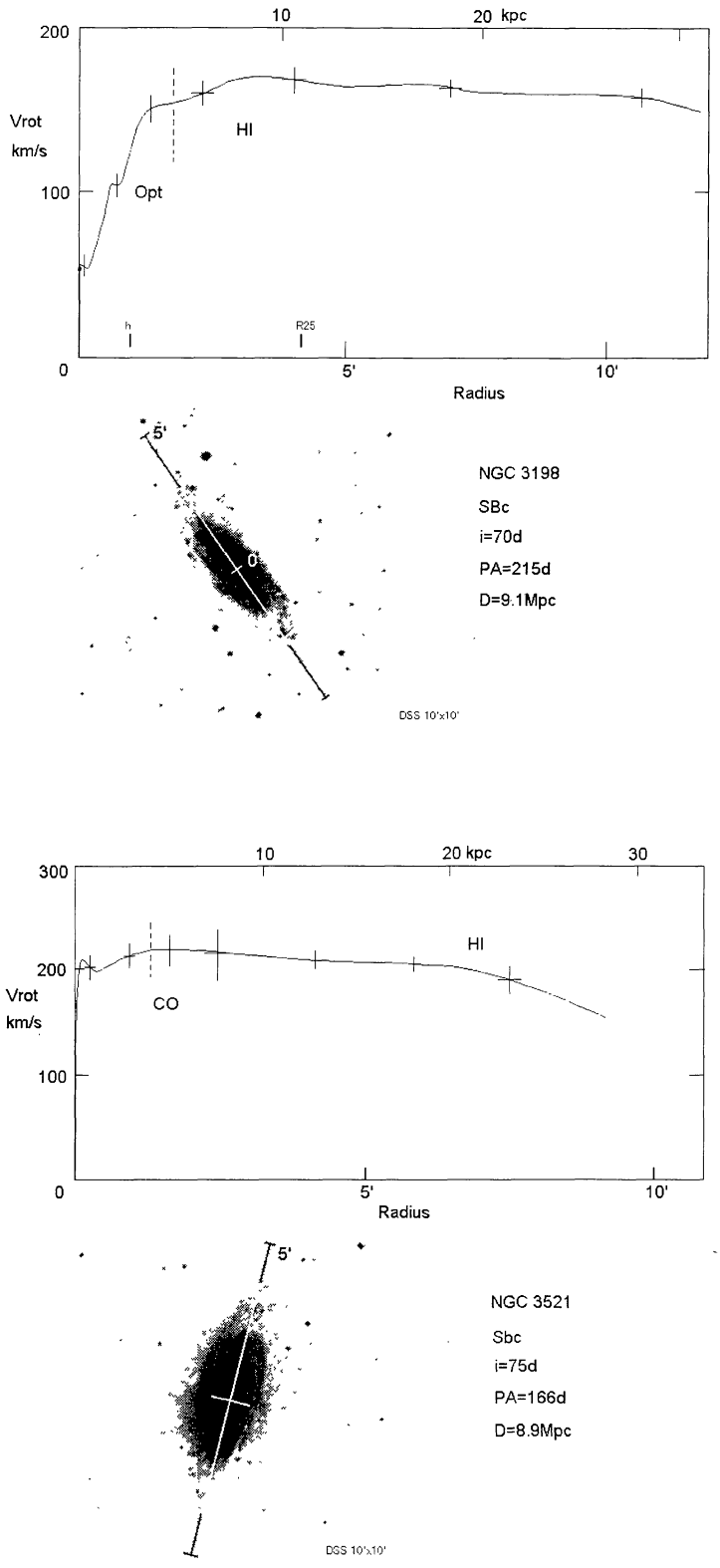

Fig. 2. (Continued)

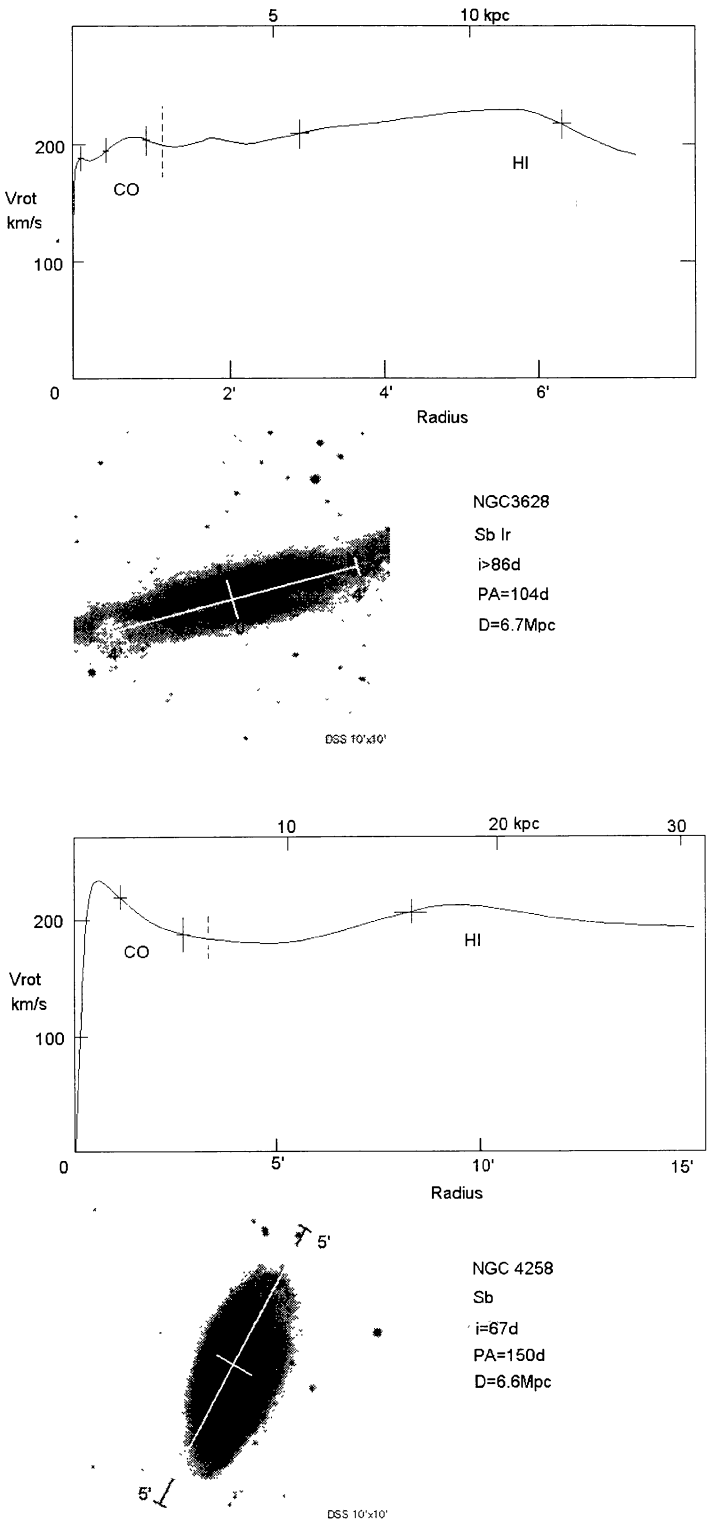

Fig. 2. (Continued)

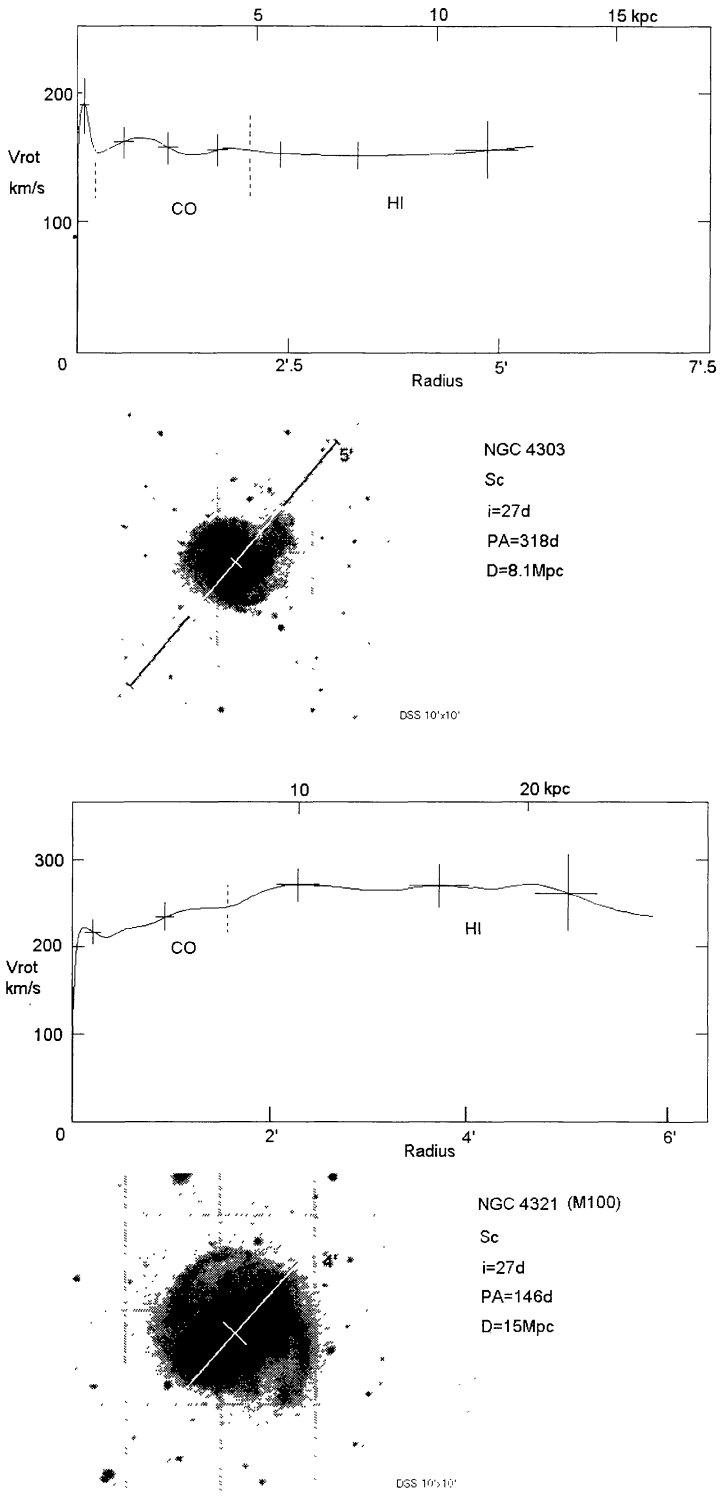

Fig. 2. (Continued)

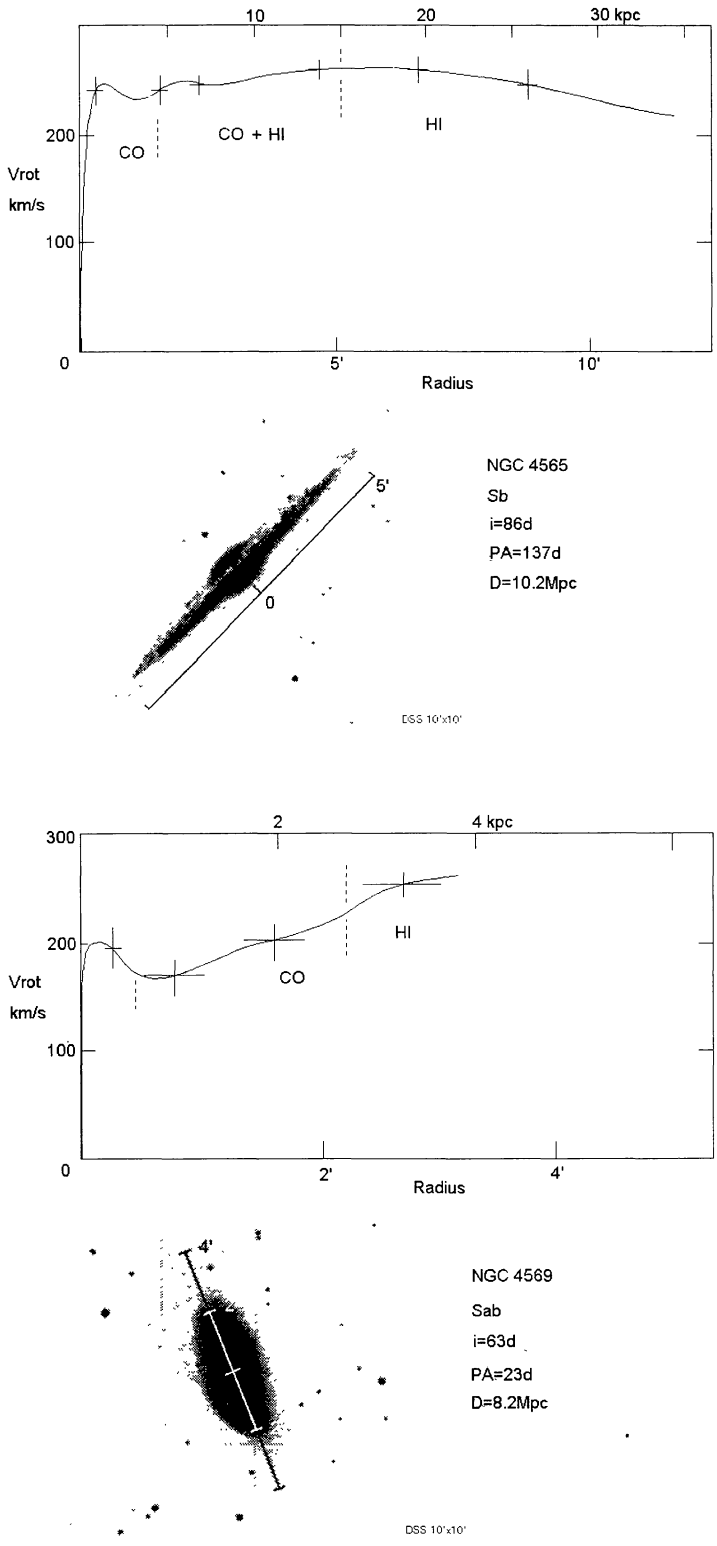

Fig. 2. (Continued)

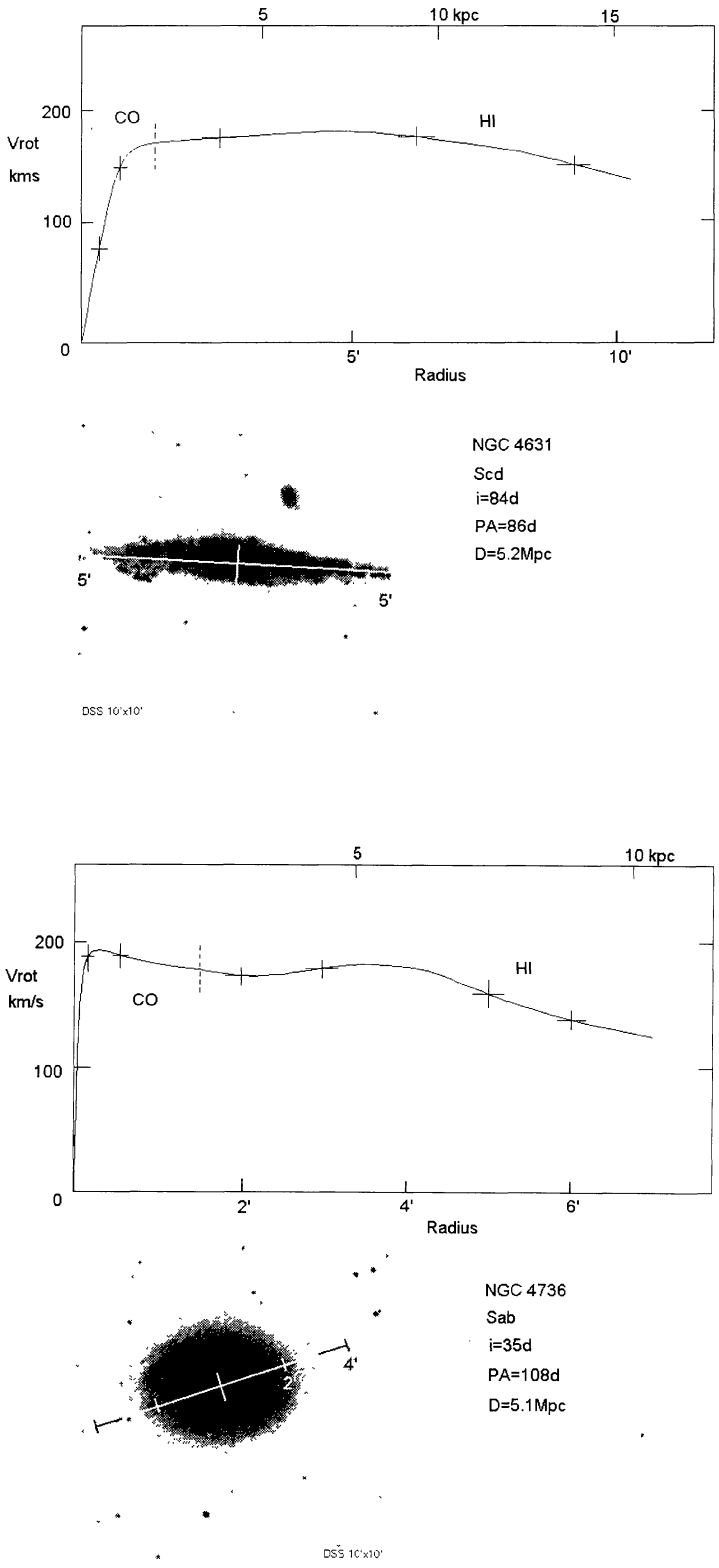

Fig. 2. (Continued)

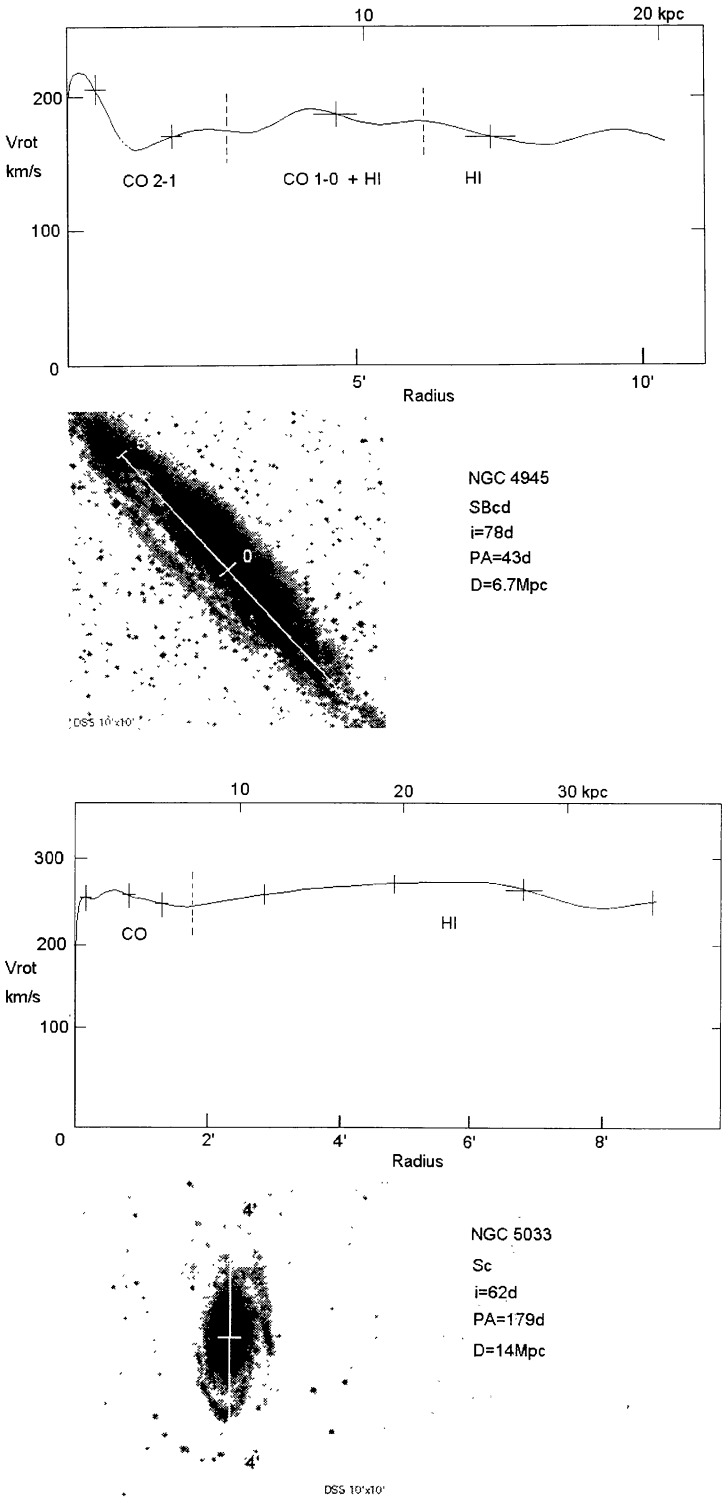

Fig. 2. (Continued)

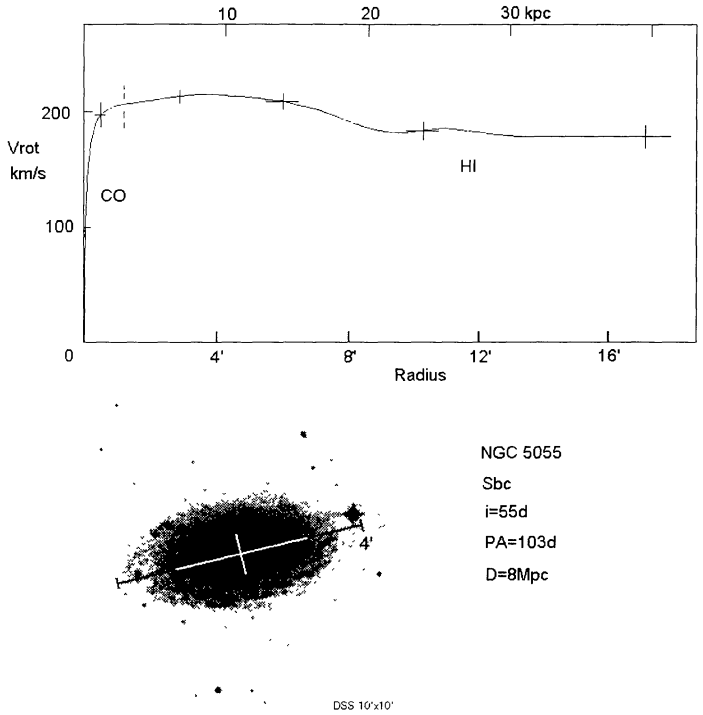

NGC 5055
Sbc
i=55d
PA=103d
D=8Mpc

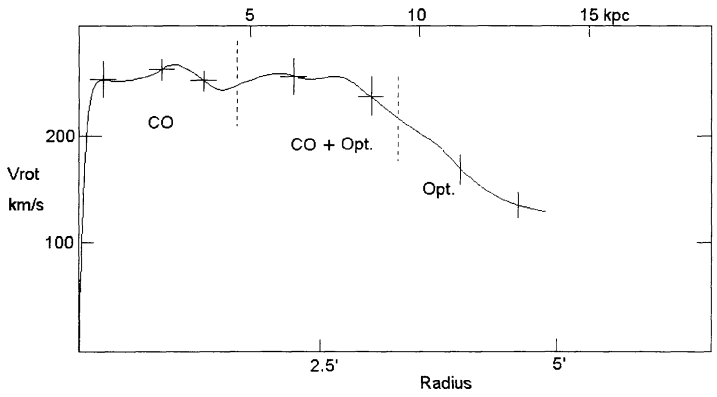

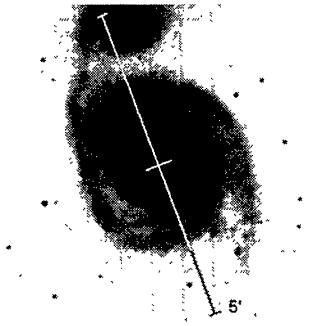

NGC 5194 (M51)
Sc
i=20d
PA=22d
D=9.6Mpc

Fig. 2. (Continued)

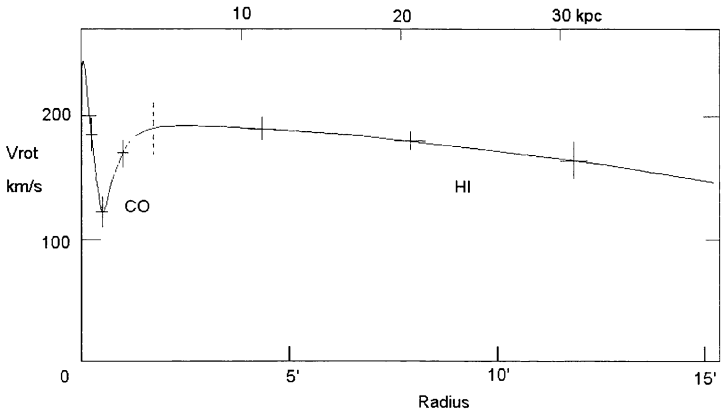

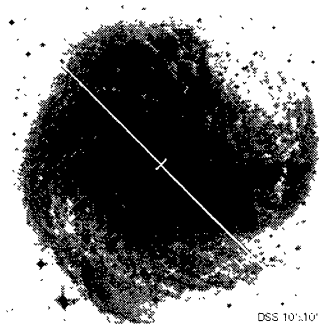

NGC 5236, M83
SBc
i=24d
PA=45d
D=8.9 Mpc

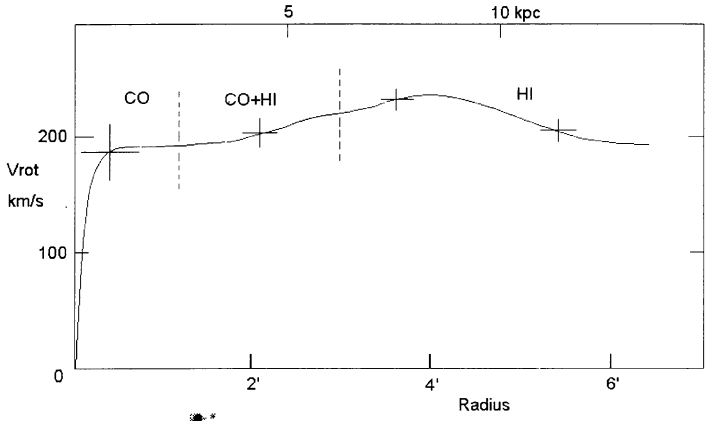

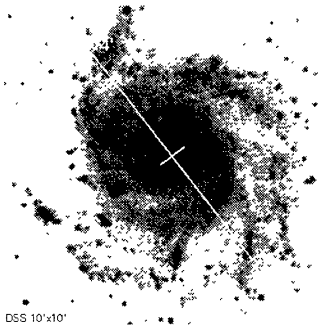

NGC 5457 (M101)
Sc
i=18d
PA=38d
D=7.2Mpc

Fig. 2. (Continued)

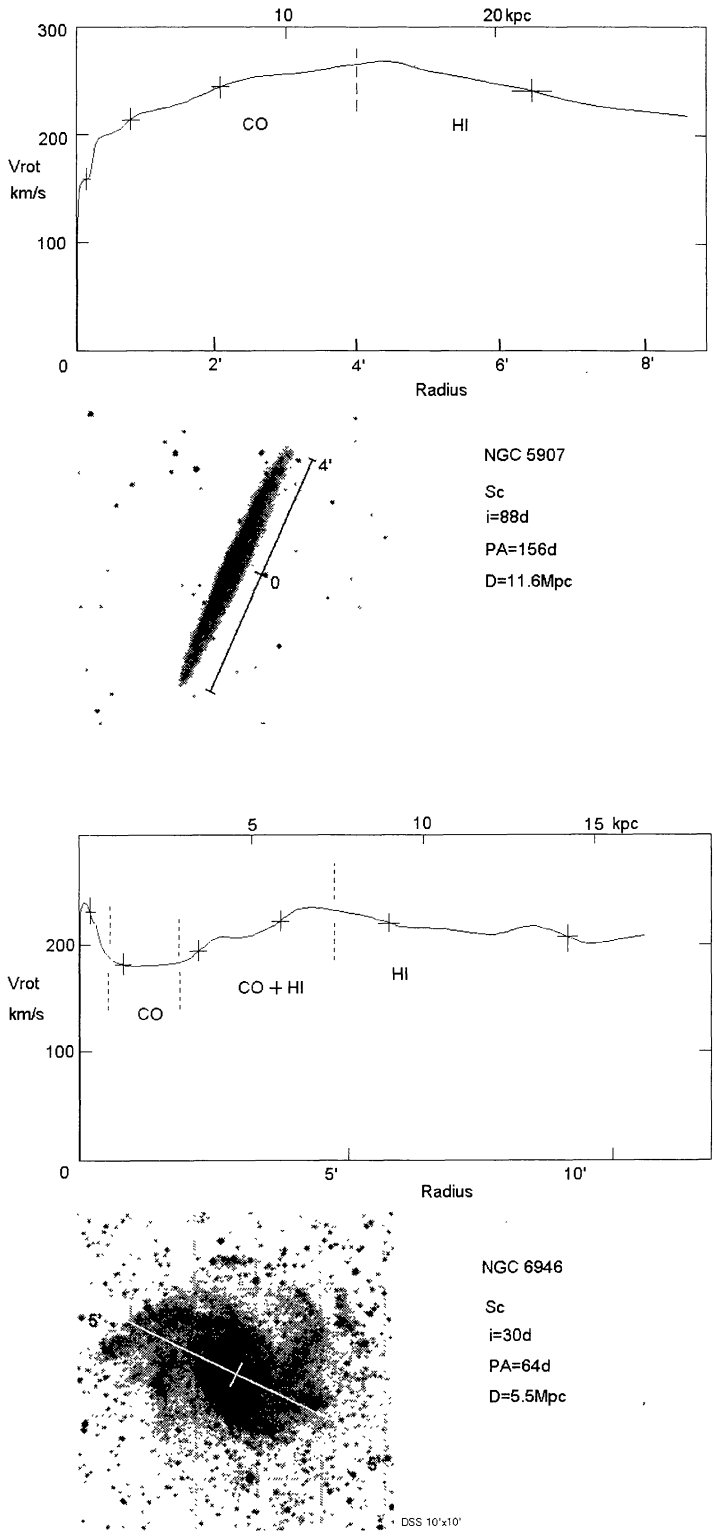

Fig. 2. (Continued)

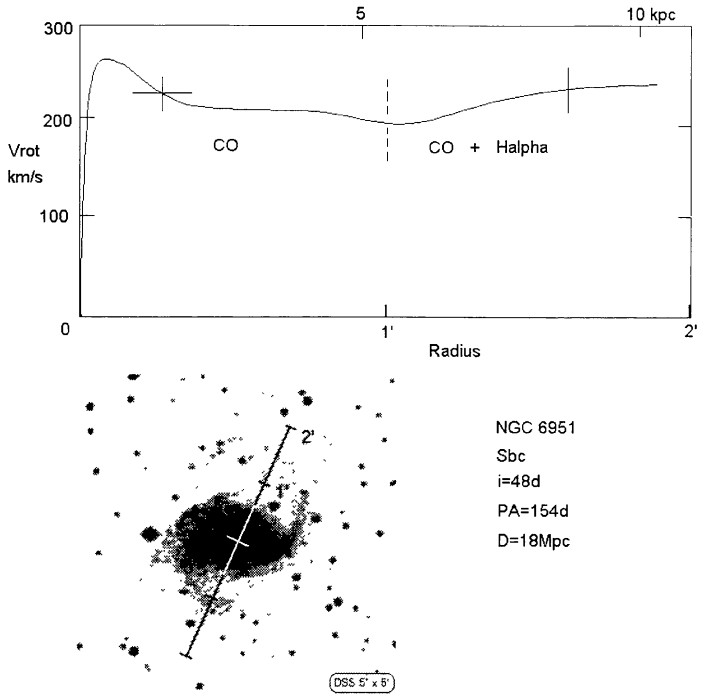

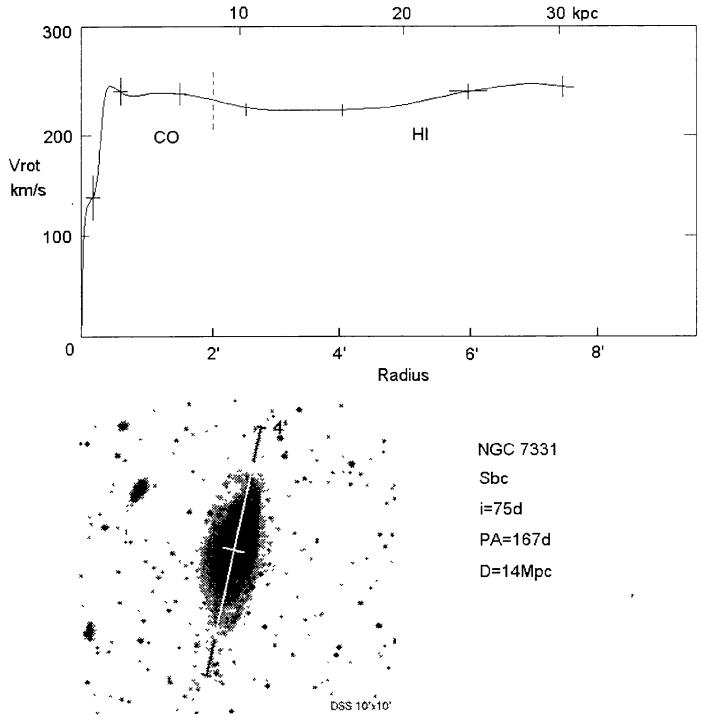

Fig. 2. (Continued)